Seamless Indoor Navigation: Leveraging AI Computer Vision and GPS Spoofing for UGV Autonomy

Stelios Ioannou
INSPIRE Research Center &
University of Lancashire (UCLan)
Pyla, Larnaca, Cyprus
SIoannou2@uclan.ac.uk

Marios Raspopoulos
INSPIRE Research Center &
University of Lancashire (UCLan)
Pyla, Larnaca, Cyprus
MRaspopoulos@uclan.ac.uk

Shilin Peng
School of Electronics and Information
Hangzhou Dianzi University
Hangzhou 310018, China
psl@hdu.edu.cn

***Abstract*—To bypass the high computational overhead and environment-specific mapping dependencies of traditional indoor localization, this work introduces a cost-effective navigation framework that enables standard autopilot controllers to operate indoors via dynamic GPS retransmission. By integrating OAK-D AI cameras for wide-area target detection with Software-Defined Radio (SDR) technology, the system generates real-time, localized GPS signals to provide seamless position inputs to commercial off-the-shelf autopilots. Experimental results demonstrate target detection with a 69% confidence floor at an operational distance of 8.5 m. Under static conditions, Kalman filtering refined the retransmitted GPS tracking accuracy from 21 cm to 13 cm within 0.6 s. Dynamic tracking trials along a complex figure-eight trajectory demonstrated that a 100 Hz non-linear EKF—fusing 5 Hz retransmitted GPS with raw IMU variable speed—effectively neutralized indoor multipath interference. This framework achieved an exceptional 2D position RMSE of just 4.28 cm, compared to a substantial 43.20 cm error yielded by a constant-speed baseline tracking architecture. This study demonstrates that dynamic GPS retransmission provides a robust, infrastructure-light alternative to complex spatial mapping, allowing standard autonomous vehicles to navigate seamlessly within GNSS-denied environments.**

Keywords*— *Indoor Navigation, Unmanned Ground Vehicle (UGV), Computer Vision, GPS Spoofing, Autonomous Navigation, SLAM, Sensor Fusion, Artificial Intelligence

I. INTRODUCTION

The evolution of the Internet of Things (IoT) and Unmanned Autonomous Systems (UAS) has intensified the demand for high-precision indoor localization, as traditional Global Navigation Satellite Systems (GNSS) suffer from signal attenuation in sheltered environments. Extensive reviews [1, 2] compare 3D indoor positioning using radio frequency and techniques such as AoA, ToA, and fingerprinting. Recent advancements in swarm UAV trajectory optimization have further utilized RSSI-based fractional-order PID (FOPID) control to navigate constrained environments effectively [3]. Alternatively, Light-based Indoor Positioning (LIP) using photodiodes and cameras [4] offers centimeter-level accuracy immune to electromagnetic interference. While these technologies provide high precision, they often lack integrated object identification and tracking.

Computer vision has bridged this gap. Image processing has achieved millimeter-range accuracy in specialized robotics, while single-camera systems have localized within known environments using PnP algorithms or Simultaneous Localization and Mapping (SLAM) for Unmanned Ground Vehicles (UGVs) [5]. Breakthroughs in Earth-fixed trajectory and map estimation have solidified the reliability of Globally Exponentially Stable (GES) SLAM filters in dynamic 3D environments [1]. Furthermore, multi-agent approaches using cooperative quadrotors have demonstrated success in industrial monitoring, such as methane emission detection, where high-precision coordination is vital [6]. Specialized robotic platforms, such as "Sewerbots," have also demonstrated that localized sensing can identify defects in complex, GPS-denied pipe networks [7].

The addition of Time-of-Flight (ToF) cameras has been shown to improve UAV positioning significantly over acoustic sensors [8]. Convolutional Neural Networks (CNN) further enhance accuracy in robotic and industrial safety applications [9]. Specifically, the algorithm, You Only Look Once (YOLO), has become the standard for real-time detection on low-power single-board computers (SBC) [10], achieving high accuracy in fire detection [11] localization [12] and vehicle tracking [13], [14]. However, multi-camera implementations often face challenges regarding camera synchronization and bounding box consistency [15].

Technical comparison of literature and the state of the art (SOTA) are tabulated on Table I.

TABLE I: TECHNICAL COMPARISON & STATE-OF-THE-ART

Ref	***Tech / Platform***	***Primary Method***	***Reported Accuracy / Performance***	***SOTA Context***
[1]	UAVs / Aerial Vehicles	GES Sensor-based SLAM	Global Convergence guaranteed; uncertainty decreases to near-zero in stationary environments	Provides an analytically proven "Globally Exponentially Stable" filter for 3D mapping

This work was co-funded by the European Union under the programme of social cohesion "THALIA 2021-2027", through Research and Innovation Foundation (Project: CONCEPT/0722/0100).

[2]	RF (WiFi/UWB)	Finger-printing	Centimeter-level (UWB) to Decimeter-level (WiFi) range	The standard benchmark for modern RF-based indoor positioning
[3]	Swarm UAVs	RSSI-based FOPID	Significant reduction in velocity tracking error; improved stability vs. standard PID	First to combine RSSI relative localization with FOPID for swarm coordination
[5]	UGVs (Ground)	SLAM (Heuristic A*)	Reduced inflection points and generation time; safe distance maintenance from obstacles	Reliable real-time mapping for unknown indoor terrestrial spaces
[6]	Multi-agent Quadrotors	Cooperative Monitoring	>99% Simulation Accuracy in formation and target tracking	High-fidelity localization specifically for industrial methane detection
[7]	Smart Sewerbot	IoT Sensing / AI	Up to 92.3% mAP for defect detection (SOTA for pipeline vision)	Addresses zero-light, high-moisture environments where GPS/RF fail
Proposed Work	AI Cameras + GPS Spoofing	YOLO + Retransmission	Centimeter precision via centralized monitoring	Achieves SOTA accuracy while using low-cost, off-the-shelf GPS autopilots

This funded research originated from Precision Agriculture (PA) applications, particularly greenhouse environments where reliable autonomous operation is essential. However, indoor greenhouse operation remains challenging due to the absence of reliable GNSS coverage.

This work addresses these limitations by proposing a cost-effective solution for indoor applications. By utilizing stationary cameras for centralized workspace monitoring and integrating AI-driven object detection with indoor GPS signal retransmission (spoofing), this system enables the dual-use of commercially available autopilots that rely on GPS for navigation. This approach provides a seamless transition for indoor agricultural operations without the need for expensive on-board computing for every vehicle.

II. METHODOLOGY AND EXPERIMENTAL SETUP

Ample aforementioned literature clearly indicated the use of cameras and radars (i.e. mmWave) for indoor positioning and navigation. However, mmWave radar hardware can only detect objects without identification, whereas AI cameras can also identify the type of object, i.e. UAV or UGV.

A. *Object Detection and Identification*

For robust object detection and identification, this work utilizes the standard YOLO algorithm. Although an optimized variant of YOLO was proposed in [11], it was excluded from this implementation because it lacks native support for the stereo vision features of the OAK-D camera system [16]. Additionally, the specific constraints targeted in [11]—namely weight, volume, and power limitations for small unmanned systems—are less critical for our stationary camera architecture. Instead, our approach prioritizes wide-area monitoring and the simultaneous 3D localization of multiple UGVs, rather than strict onboard processing restrictions.

The training dataset was developed and managed using Roboflow [17], which streamlined image annotation, preprocessing, and augmentation. This platform ensured that the exported data was fully compatible with the YOLO architecture, enabling efficient model training tailored to our specific indoor environment. To evaluate performance, the dataset was randomly partitioned into three independent, distinct sets:

- Training set: 83% of the images (20,255)
- Validation set: 13% of the images (3,148)
- Test set: 4% of the images (977)

B. *Distance Calculation using AI Camera*

The OAK-D (OpenCV AI Kit) calculates depth via stereo vision using two identical, side-by-side monochrome global shutter cameras. By capturing slightly offset views of the same scene, the system performs stereo matching to identify corresponding pixels. The fundamental principle behind this calculation is triangulation. As shown in Figure 1, the depth distance (Z) is derived from the focal length (*f*), the baseline distance between cameras (B), and the disparity (*d*). For this camera B=7.5cm.

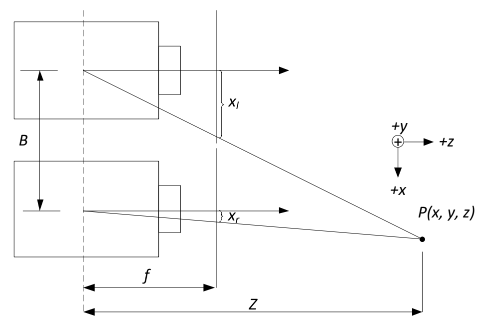

Figure 1: Triangulation geometry for 3D depth estimation.

The relationship is expressed mathematically as:

$$Z = \frac{fB}{d} = \frac{fB}{X_l - X_r} \tag{1}$$

The disparity (*d*) is the difference in horizontal coordinates (x_l - x_r) between matching pixels. The positions where the projection lines hit the left and right image planes are denoted by x_l and x_r respectively. From the resulting 3D coordinates (x, y, z), the horizontal (θ_x) and vertical (θ_y) angles between the camera and the target are calculated geometrically using:

$$\theta_x = \arctan\left(\frac{x}{z}\right) \tag{2}$$

$$\theta_y = \arctan\left(\frac{y}{z}\right) \tag{3}$$

Stereo depth mapping in OpenCV typically utilizes two primary algorithms: STEREO_BM (Block Matching) and STEREO_SGBM (Semi-Global Block Matching). Both require rectified image pairs to ensure scanline alignment.

To ensure precision, the OAK-D undergoes a calibration phase using a known pattern (typically a chessboard) to correct for lens distortion. The camera utilizes a hardware-accelerated Semi-Global Matching (SGM) algorithm to compute disparities. The resulting grayscale disparity map is then converted into a metric depth map, providing the real-world distance of every point in the scene relative to the camera sensors.

C. Indoor Positioning and Navigation

It is well known that GPS is for outdoor applications. For indoor or covered areas, the signal is obstructed and blocked and the GPS based systems do not work.

This research proposes a system where the unmanned systems, UGV and UAV, will be first detected by a camera system and then their local indoor location within the 3D space will be calculated. When the local coordinates are calculated then they will be converted to the GPS coordinate system and retransmitted. This is also known as "GPS spoofing". The GPS retransmission/spoofing will not in any way interfere with the original GPS signals because they are obstructed and blocked already by the building structures. The main reason this research proposes the retransmission of GPS signals is for indoor navigation using commercially available controllers and autopilots. For example, a commercially available UAV such as the DJI Mavic 3M will still navigate because the GPS signal will be available. Other available hardware includes but are not limited to Ardupilot AMP2.5 autopilot and Arduino based controllers.

The software defined radio (SDR), HackRF One, was used for GPS retransmission. For static and dynamic retransmissions, the software list includes GPS-SDR-SIM, visual studio, Pothos SDR, SatGen V3 and the latest RINEX navigation ephemerides broadcast brdc file from NASA [18].

D. State Estimation and Data Fusion Strategy

To mitigate the inherent noise in the OAK-D's spatial coordinates and the GPS receiver's jitter, a discrete-time Kalman Filter (KF) was implemented. The filter serves as an optimal estimator by recursively minimizing the mean square error of the object's position. The algorithm operates in a two-step recursive process: Prediction and Correction. The state of the system at time k is represented by the vector $\boldsymbol{s}_k$.

To achieve high-precision indoor navigation, the system employs a two-stage filtering architecture. This approach separates the stationary noise-reduction task (stationary) from the dynamic sensor fusion task (motion).

1) Stationary Phase: Constant Position KF (5Hz)

When the UGV is stationary, a discrete-time Kalman Filter (KF) acts as an optimal recursive averager to mitigate OAK-D spatial coordinate noise and GPS jitter. The state is defined as $\mathbf{s}_k = [x, y, z]^T$ with the state transition matrix $\boldsymbol{F} = \boldsymbol{I}$ (3X3 identity matrix). The filtering process minimizes the mean square error through the standard Prediction and Correction cycle:

Prediction - The prediction process includes time update where the filter projects the current state and error covariance P forward in time.

$$\hat{\boldsymbol{s}}_k^- = \boldsymbol{F}\hat{s}_{k-1} \tag{4}$$

$$\boldsymbol{P}_k^- = \boldsymbol{F}\boldsymbol{P}_{k-1}\boldsymbol{F}^T + \boldsymbol{Q} \tag{5}$$

Correction (Measurement Update): Following the prediction, the filter performs a measurement update, where the state estimate is refined based on the observed data z_k (e.g., OAK-D spatial coordinates or GPS data). This step adjusts the predicted state by calculating the Kalman Gain $\mathbf{K}_k$, which weights the importance of the new measurement relative to the uncertainty in the model.

The mathematical implementation is as follows:

Kalman Gain Calculation:

$$\boldsymbol{K}_k = \boldsymbol{P}_k^-\boldsymbol{H}^T(\boldsymbol{H}\boldsymbol{P}_k^-\boldsymbol{H}^T + \boldsymbol{R})^{-\mathbf{1}} \tag{6}$$

State Update:

$$\hat{\mathbf{s}}_k = \hat{\mathbf{s}}_k^- + \boldsymbol{K}_k(\boldsymbol{z}_k - \boldsymbol{H}\hat{\mathbf{s}}_k) \tag{7}$$

Covariance Update:

$$\boldsymbol{P}_k = (\boldsymbol{I} - \boldsymbol{K}_k\boldsymbol{H})\boldsymbol{P}_k^- \tag{8}$$

For stationary scenario, the system was modeled using a *Constant Position* assumption where the state transition matrix **F** is the identity matrix, **I**. In addition, the process noise Q is set to a near-zero value (i.e. 10^{-6}), and the measurement noise **R** is configured to match the observed variance of the GPS receiver. Under these conditions, the Kalman Gain **K** decreases over time, allowing the filter to converge on the true coordinate by acting as an "*optimal recursive averager*".

2) Dynamic Phase: 3D Extended Kalman Filter (100Hz)

When the UGV is in motion, the system transitions to an Extended Kalman Filter (EKF). This phase is designed to fuse high-frequency IMU dead-reckoning with vision-based positioning at a rate of 100Hz. To accommodate full 3D indoor operation, the state vector is expanded to include both position and velocity:

$$\boldsymbol{s}_k = [x, y, z, \dot{x}, \dot{y}, \dot{z}]^T \tag{9}$$

The system assumes a Constant Velocity (CV) model between time steps. To project the state forward, we define the state transition matrix F (6X6). This matrix uses the sampling interval Δt (where Δt = 0.01s for a 100Hz update rate) to link velocity to position:

$$F = \begin{bmatrix} I_3 & \Delta t I_3 \\ 0_3 & I_3 \end{bmatrix} \tag{10}$$

Prediction and Linearization: Since the UGV's motion in an indoor environment is inherently nonlinear, the EKF employs a first-order Taylor expansion to linearize the system at each time step. The Prediction (Time Update) step projects both the state estimate and the error covariance $\boldsymbol{P}$ forward in time.

State Prediction: The next state is estimated using the nonlinear motion model *f(.)* which accounts for the UGV's kinematics:

$$\hat{\mathbf{s}}_k^- = f(\hat{s}_{k-1}, u_{k-1}) \tag{11}$$

Covariance Prediction: To propagate uncertainty, the nonlinear model is linearized by calculating the Jacobian matrix F_k:

$$F_k = \frac{\partial f}{\partial s}|_{\hat{s}_{k-1}} \tag{12}$$

The error covariance is then updated as:

$$\boldsymbol{P}_k^- = \boldsymbol{F}_k \boldsymbol{P}_{k-1} \boldsymbol{F}^T + \boldsymbol{Q} \tag{13}$$

While the stationary phase assumes a static state ($F=I$), the dynamic phase utilizes the generalized covariance prediction (12), where F_k propagates the uncertainty through the UGV's motion model.

III. Experimental Results

A. Experimental Setup / Implementation Section

To validate the framework, a hardware testbed was established using a HackRF One SDR with a 0.5 ppm TCXO for carrier stability. The signal generation toolchain integrated *gps-sdr-sim*, Visual Studio, Pothos SDR, SatGen V3, and daily NASA CDDIS broadcast RINEX files [18]. To ensure autopilot acquisition without receiver saturation, the SDR was configured to the GPS L1 band (1575.42 MHz) at a baseband sampling rate of 2.6 MSps using a 16-bit signed integer format; hardware TX gain was set to -12 dB alongside a 40 dB inline coaxial attenuator to deliver approximately -130 dBm over-the-air signal power. While static states relied on pre-compiled coordinates, dynamic testing utilized a real-time UDP stream updating coordinates at 5 Hz. The discrete-time EKF executed at 100 Hz ($\Delta t = 0.01$ s). Based on physical sensor noise profiles, the filters were initialized with an experimental position tracking variance of σ = 1.0 m across all axes, yielding a measurement noise covariance of R = diag(1.0, 1.0, 1.0) m^2. Driven by the IMU accelerometer (σ_{acc} = 0.1m/s^2) and gyroscope (σ_{gyro} = 0.05 rad/s) noise floors, the structural velocity error variance over Δt was established as $\sigma^2 = (\sigma_{acc}\,\Delta t)^2 = 10^{-6}$ m/s^2 and the position tracking variance was bounded to a stable numerical minimum of 10^{-8} m^2 defining the process noise covariance matrix as Q = diag (10^{-8}, 10^{-8}, 10^{-8}, 10^{-6}, 10^{-6} 10^{-6}).

B. Sensitivity Analysis and Detection Limits

The sensitivity analysis presented in Fig. 2 evaluates the YOLO algorithm's performance under varying lighting conditions, specifically identifying the minimum pixel footprint required for robust object detection. Findings demonstrate that detection confidence is inversely proportional to the distance of the object from the sensor.

As evidenced in Fig. 3 (a) the YOLO algorithm maintains a robust detection confidence exceeding 68% even at a distance of 7.5m whereas detection confidence scales significantly Fig. 3 (b) with object size and proximity (bigger bounding box): the system achieves 98% confidence for larger objects at 2.7m. These results confirm that the system effectively differentiates the target object from complex, high-clutter backgrounds, even when target and environmental color profiles are closely matched. Furthermore, these findings suggest the algorithm is capable of reliable operation beyond 10m, though experimental verification was limited by the 8m laboratory environment.

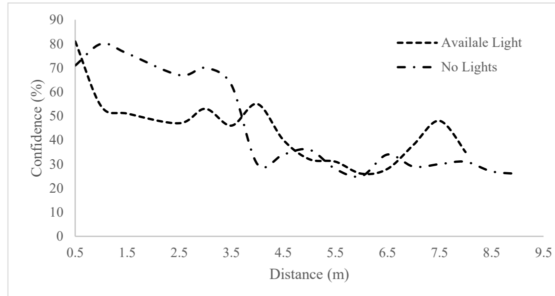

Fig 2: Sensitivity Analysis – Object Detection and Identification as a Function of Distance

As illustrated in Figs. 4 (a) and (b), the algorithm robustly identifies multiple objects simultaneously, despite significant environmental clutter. Detected targets are localized via bounding boxes and assigned corresponding labels. While experimental validation was limited to three simultaneous objects due to resource availability, existing literature indicates that the YOLO architecture is not constrained by the number of detectable objects

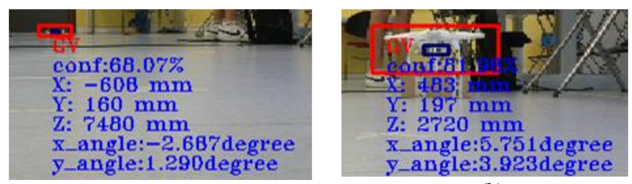

(a) *(b)*

Fig 3: Object Detection and Identification

(a)
Birdseye View

(b)
Profile View

Fig 4: Simultaneous Multiple Object Detection and Identification

C. Indoor Positioning using AI Camera

As illustrated in Fig. 5, the system achieves high precision across all axes, with average errors of 9.0 cm in the *x*-direction, 1.9 cm in the *y*-direction, and 4.5 cm in the *z*-direction. The cumulative 3D average error, which accounts for transient estimation fluctuations, is 21.8 cm. These sub- decimeter accuracies in the lateral and vertical axes compare favorably against current state-of-the-art localization algorithms. Notably, this level of performance is achieved without prior map data, demonstrating the system's robustness in unknown, dynamic indoor environments.

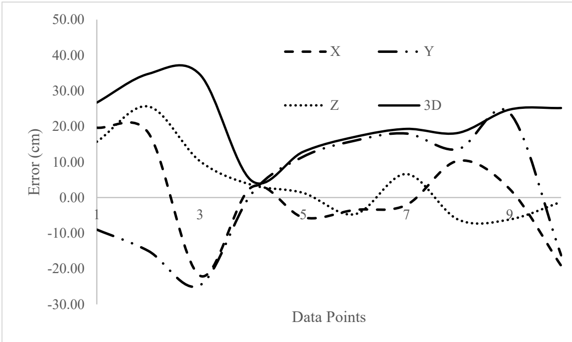

Fig 5: Error (cm) for Calculated Distance from AI Camera

D. Signal Isolation and GPS Injection

To establish a controlled indoor testing environment, we first verified the absence of external GPS signals at the laboratory coordinates (35º00'30"N, 33º41'48'E). Signal isolation was confirmed using both a spectrum analyzer and by verifying that standard controllers including ArduPilot and DJI failed to achieve a GPS lock. Then, an SDR-based injection strategy was implemented to simulate GPS availability. Using HackRF One, a GPS signal was injected / retransmitted into the environment. As shown in Fig. 6, the injected frequency was successfully detected by the spectrum analyzer, and all test units subsequently achieved stable GPS locks, validating the testbed for spoofing analysis.

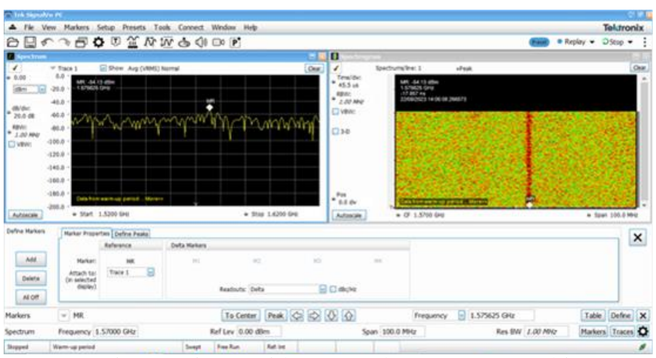
Fig 6: Verification of successful GPS signal retransmission and frequency alignment using a spectrum analyser

1) Static GPS Spoofing Analysis

Fig. 7 illustrates the GPS signal acquisition under static conditions, where the transmitted GPS data exhibits high precision but significant bias—rendering the received coordinates inaccurate. By applying the Kalman Filter (KF) as an optimal recursive averager, the system successfully filters the biased signal and converges to the true laboratory coordinate. This confirms the filter's efficacy in mitigating systematic positioning offsets common in spoofed or retransmitted environments.

The accuracy of the GPS signal post-filtering is illustrated in Fig. 8. The filter demonstrates rapid convergence: the positional error is reduced to 19 cm within 0.5 s, improves to 13 cm within 0.6 s, and achieves sub-centimeter convergence within 1.0 s. These results quantify the filter's capability to restore positioning reliability even when the source data is compromised.

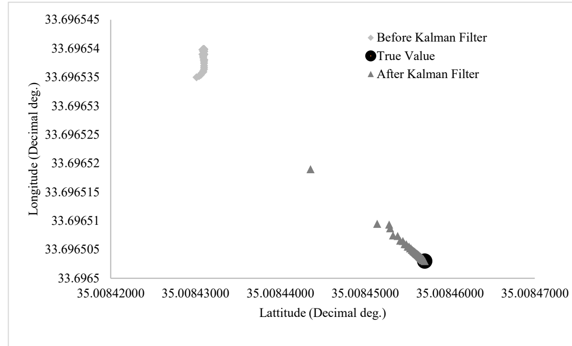

Fig 7: Static GPS Convergence after Kalman Filtering

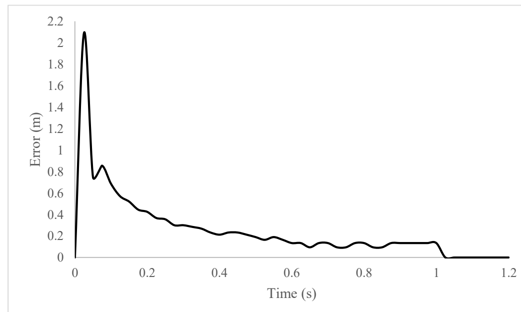

Fig 8: Error (cm) Received GPS after Kalman Filtering

E. Dynamic Navigation and Trajectory Tracking

System performance was evaluated across nine waypoints in a dynamic figure-eight trajectory (Figs. 9 and 10) to challenge UGV maneuverability and heading accuracy. While an Arduino handled low-level actuator timing, its computational limits required routing state-estimation frameworks to a Raspberry Pi 4 (2 GB RAM) for uniform execution at 100 Hz ($\Delta t = 0.01$s).

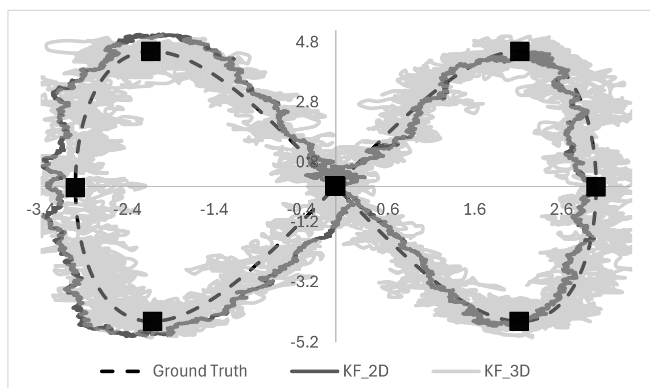

Fig 9: Comparison of KF and EKF, Constant Speed at 100Hz

Benchmarking under this unified update rate isolated the localization impact of motion constraints:

- 3D Linear KF (Constant Speed, 100 Hz) of Fig 9: Expanding the state space into three dimensions introduced an unconstrained vertical (Z) estimation channel. On a flat laboratory floor where vertical motion is absent, this extra degree of freedom allowed unmodeled noise to propagate into the horizontal states, resulting in an increased 2D position RMSE of 43.20 cm.

- 2D Linear KF (Constant Speed, 100 Hz) of Fig 9: By explicitly ignoring the vertical axis and restricting the state space to the planar motion of the UGV, this model eliminated out-of-plane noise coupling. Even under a constant-speed limitation, it achieved a superior tracking accuracy with an RMSE of 33.93 cm.
- High-Frequency EKF (Variable Speed, 100 Hz) of Fig 10: Achieving an exceptional RMSE of 4.28 cm, this architecture actively integrated high-frequency IMU accelerometer ($\sigma_{acc} = 0.1$ m/s^2) and gyroscope ($\sigma_{gyro} = 0.05$ rad/s) data to propagate true variable speed.

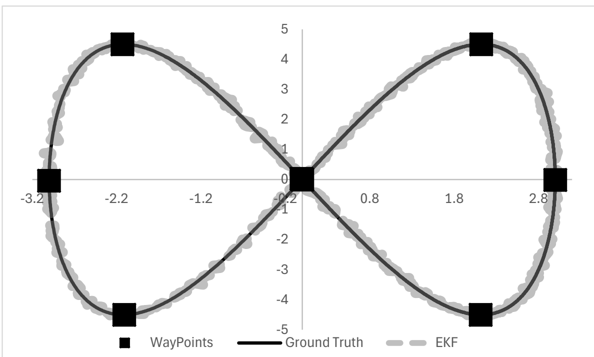

Fig 10: EKF Variable Speed at 100Hz

As shown in Fig. 10, the 100 Hz variable-speed EKF effectively anchored tracking between sparse 5 Hz GPS updates, mitigating laboratory multipath interference and proving that physical kinematic modeling dictates sub-decimeter indoor accuracy far more than raw sampling frequency.

IV. Conclusions

This research presents a cost-effective indoor navigation framework integrating off-the-shelf OAK-D AI cameras for target detection, SDRs for GPS retransmission, and standard autopilot architectures. High-frequency estimation bottlenecks were resolved via a distributed computing topology assigning low-level timing to an Arduino and primary 100 Hz estimation toolchains to a Raspberry Pi 4. Empirical results show that the OAK-D camera reliably tracks targets with 69% confidence at 8.5m. Benchmarking at 100 Hz demonstrated that proper structural motion modeling heavily mitigates localization drift; the IMU-driven variable-speed EKF achieved a 4.28 cm position RMSE, vastly outperforming the constant-speed 3D Linear KF (33.93 cm) and Standard EKF (43.20 cm). Furthermore, spoofing profiles confirmed that the EKF resolves retransmitted GPS biases to restore sub-decimeter fidelity within 1.0 s.

Future work will deploy multi-camera triangulation arrays and benchmark this SDR framework against literature-established radar localization systems [19-21] regarding real-time latency and accuracy boundaries.

V. References

[1] P. Lourenço, B. J. Guerreiro, P. Batista, P. Oliveira, and C. Silvestre, “Earth-fixed trajectory and map online estimation: Building on GES sensor-based SLAM filters,” Robotics and Autonomous Systems, vol. 130, p. 103552, 2020, doi: 10.1016/j.robot.2020.103552

[2] A Sesyuk, S Ioannou and M Raspopoulos, “A Survey of 3D Indoor Localization Systems and Technologies”, Sensors 22 (23), 9380, 2022.

[3] G. E. M. Abro, “Trajectory optimisation for swarm UAVs in constrained environments with RSSI-based FOPID control,” Discover Electronics, vol. 2, no. 1, p. 77, 2025.

[4] M. Maheepala, A. Z. Kouzani and M. A. Joordens, "Light-Based Indoor Positioning Systems: A Review", IEEE SENSORS JOURNAL, VOL. 20, NO. 8, APRIL 15, 2020.

[5] N. U. Rehman and K. Kumar, “Implementation of an autonomous path planning & obstacle avoidance UGV using SLAM,” in Proc. 2018 Int. Conf. Eng. Emerging Technol. (ICEET), 2018, pp. 1–5.

[6] G. E. M. Abro, A. M. Abdallah, and I. Al Jalal, “Multi-agent approach for methane emission monitoring from an industrial facility using cooperative quadrotor unmanned aerial vehicles,” in Proc. 2024 IEEE 9th Int. Conf. Eng. Technol. Appl. Sci. (ICETAS), 2024, pp. 1–4.

[7] G. E. M. Abro, B. Jabeen, K. K. Ajodhia, A. Rauf, and A. Noman, “Designing smart sewerbot for the identification of sewer defects and blockages,” Int. J. Adv. Comput. Sci. Appl., 10, 2, pp.615–619, 2019.

[8] J. A. Paredes, F. J. Álvarez, T. Aguilera nd J. M. Villadangos, "3D Indoor Positioning of UAVs with Spread Spectrum Ultrasound and Time-of-Flight Cameras", Sensors 18, 89, 2018.

[9] J. Miseikis et al., "Robot Localisation and 3D Position Estimation Using a Free-Moving Camera and Cascaded Convolutional Neural Networks," in Proc. IEEE/ASME Int. Conf. Adv. Intell. Mechatronics (AIM), Auckland, New Zealand, 2018, pp. 181–187.

[10] H. Feng et al., "Benchmark Analysis of YOLO Performance on Edge Intelligence Devices," Cryptography, vol. 6, no. 2, p. 16, Jun. 2022.

[11] J. Ye, S. Ioannou, P. Nikolaou and M. Raspopoulos, "CNN based Real-time Forest Fire Detection System for Low-power Embedded Devices", The 31st Mediterranean Conference on Control and Automation (MED2023), 2023.

[12] R. R. Nori, R. N. Farhan, and S. H. Abed, "Indoor and Outdoor Fire Localization Using YOLO Algorithm," J. Phys.: Conf. Ser., vol. 2114, no. 1, p. 012067, Dec. 2021.

[13] M. Vajgl, P. Hurtik, and T. Nejezchleba, "Dist-YOLO: Fast Object Detection with Distance Estimation," Appl. Sci., vol. 12, no. 3, p. 1354, Jan. 2022.

[14] R. Waranusast, P. Riyamongkol, and P. Pattanathaburt, "Distance Estimation Between Camera and Vehicles from an Image using YOLO and Machine Learning," in Proc. Asia-Pacific Signal Inf. Process. Assoc. Annu. Summit Conf. (APSIPA ASC), Chiang Mai, Thailand, 2022, pp. 482–488.

[15] G. Kulathunga, A. Buyval, and A. Klimchik, "Multi-Camera Fusion in Apollo Software Distribution," IFAC-PapersOnLine, vol. 52, no. 8, pp. 49–54, 2019.

[16] Luxonis “OAK-D”, Online Posting: https://shop.luxonis.com/products/oak-d?srsltid=AfmBOorqeikc01QRsEUzhlmS-dZ0TZSjSU2e3l5Zzu8t-g3cD_DEH1Rf [Accessed 17/04/2025].

[17] Roboflow, “Everything you need to build and deploy computer vision applications”, Online Application: https://roboflow.com/ [Accessed 17/4/25].

[18] NASA, “Latest RINEX navigation ephemerides broadcast brdc file”, Online: https://cddis.nasa.gov/archive/gnss/data/daily/2023/brdc/ [Accessed 17/04/2025].

[19] A.Sesyuk, S. Ioannou and M. Raspopoulos, “3D millimeter-Wave Sensing vs Ultra-wideband Positioning¨, The 14th International Conference on Indoor Positioning and Indoor Navigation 2024 (IPIN 2024), Hong Kong, 2024.

[20] A.Sesyuk, S. Ioannou and M. Raspopoulos, “Radar-based millimeter-Wave sensing for accurate 3D Indoor Positioning - Potentials and Challenges”, IEEE Journal on Indoor Seamless Positioning and Navigation, 2024.

[21] A Sesyuk, S Ioannou and M Raspopoulos, “3D millimeter-Wave Indoor Localization”, 13th International Conference on Indoor Positioning and Indoor Navigation (IPIN), Germany, 2023.